Optimized energy landscape exploration using the *ab initio* based activation-relaxation technique

Eduardo Machado-Charry,[1,2,a)] Laurent Karim Béland,[3] Damien Caliste,[2]
Luigi Genovese,[2] Thierry Deutsch,[2] Normand Mousseau,[3,b)] and Pascal Pochet[2,c)]

[1]*Nanosciences Foundation, 23 rue des martyrs, 38000 Grenoble, France*
[2]*Laboratoire de simulation atomistique (L_Sim), SP2M, UMR-E CEA/UJF-Grenoble 1, INAC, Grenoble, F-38054, France*
[3]*Département de Physique and Regroupement Québécois sur les Matériaux de Pointe (RQMP), Université de Montréal, C.P. 6128, Succursale Centre-Ville, Montréal, Québec H3C 3J7, Canada*

Unbiased open-ended methods for finding transition states are powerful tools to understand diffusion and relaxation mechanisms associated with defect diffusion, growth processes, and catalysis. They have been little used, however, in conjunction with *ab initio* packages as these algorithms demanded large computational effort to generate even a single event. Here, we revisit the activation-relaxation technique (ART nouveau) and introduce a two-step convergence to the saddle point, combining the previously used Lanczós algorithm with the direct inversion in interactive subspace scheme. This combination makes it possible to generate events (from an initial minimum through a saddle point up to a final minimum) in a systematic fashion with a net 300–700 force evaluations per successful event. ART nouveau is coupled with BigDFT, a Kohn-Sham density functional theory (DFT) electronic structure code using a wavelet basis set with excellent efficiency on parallel computation, and applied to study the potential energy surface of C_{20} clusters, vacancy diffusion in bulk silicon, and reconstruction of the 4H-SiC surface. © *2011 American Institute of Physics*. [doi:10.1063/1.3609924]

I. INTRODUCTION

The effective identification of activated diffusion pathways has been a major concern for a long time in condensed matter, physical chemistry, and materials science, and many methods have been developed over the years to tackle this issue. When both the initial and final states are known, most approaches work by optimizing an initially guessed pathway connecting these two states. This is the basis for the nudge-elastic band method[1] (NEBM) and its variants[2,3] as well as algorithms, such as the growing string method.[4–6]

When only one state is known, open-ended methods, such as activation-relaxation technique (ART) (Ref. 7) and ART nouveau,[8] as well as the eigenvector-following,[9] the dimer method,[10] the minima hopping method,[11] and the global reaction route mapping[12] are necessary. These algorithms all work by deforming the initial minimum in order to find an unstable direction that can be followed up to a first-order saddle point, characteristic of a transition state. This family of methods has been used to predict and identify transition states in a number of systems ranging from atomic clusters to disordered materials and proteins.[8,13–16] They have proven reliable and efficient when coupled with empirical potential.[8,13–16]

In general, open-ended methods have been much less used with *ab initio* potentials. Even though some widely distributed codes include such methods (e.g., the dimer method

is available in VASP (Ref. 17) and ART nouveau for SIESTA (Refs. 18–20)) the large number of force evaluations required to converge to a nearby saddle point has limited its application.

Building on a recent characterization of ART nouveau,[21] we propose here a series of improvements that increase significantly the efficiency of the algorithm in terms of computational power required per event while offering a much stricter convergence to the transition state. These modifications allow us to sample efficiently the configuration space of a number of systems—molecules, bulk and surfaces—in a controlled manner that opens up the possibility of generalizing the use of this approach to a wider range of problems that requires the *ab initio* accuracy.

The paper is organized as follows. In Sec. II, we present a brief description of the activation-relaxation technique. Afterwards, we present a way to accelerate the convergence to the saddle point using the direct inversion in interactive subspace (DIIS) scheme. In Sec. III, we show the capabilities of this methodology in the exploration of the energy landscape of molecules, here C_{20}, crystals, a vacancy in crystalline silicon (c-Si) and surfaces, by looking at the $(2 \times 2)_C$ reconstruction of 4H-SiC.

II. METHODOLOGY

The exploration of the potential energy surface (PES) of a N-particle system by ART requires a continuous description provided in terms of forces and energy. For atomic systems, these quantities can be calculated at various approximation levels, ranging from *ab initio* to semi-empirical and empirical.

---
a)URL: http://inac.cea.fr/L_Sim.
b)Electronic mail: normand.mousseau@umontreal.ca. URL: http://www.phys.umontreal.ca/mousseau.
c)Electronic mail: pascal.pochet@cea.fr.

While ART nouveau has been mostly used with empirical potentials,[8,13–15] a first integration with the SIESTA package,[18] a local basis *ab initio* method, was proposed in 2004, following a similar implementation with the eigenvector-following method.[16] Although SIEST-A-RT (Ref. 19) proved sufficiently efficient for the characterization of vacancy diffusion in various systems,[20,22] the number of force evaluations required in the original ART nouveau implementation remained too high for its systematic use in problems requiring a description at *ab initio* level.

In this paper, we present a more stringent implementation of ART nouveau, coupled with the recently proposed *ab initio* method BigDFT.[23] This latter method uses a systematic wavelet basis set with high convergence properties, very good performances, and an excellent efficiency for parallel calculations including hybrid parallel architecture with graphic processing units (GPU).[24] BigDFT is, therefore, very attractive for dealing with complex and large systems. Since we focus here on improvements to ART nouveau, we refer the reader to Ref. 23 for a complete description of the BigDFT method.

Contrary to methods, such as basin-hopping,[25] that sample very efficiently the configurations of complex systems, ART is a method for constructing trajectories on the energy landscape of activated systems, with not only minima but also transition states. Instead of following in detail the thermal fluctuations, it searches directly for transition states characterized as first-order saddle points in the energy landscape. This method was proposed by Barkema and Mousseau[13] and then refined by Malek and Mousseau as ART nouveau[8] to ensure a controlled convergence to the saddle point. A recent characterization of its various parameters and a discussion on how to optimize the original algorithm can be found in Ref. 21.

An ART event can be summarized in three stages.

(1) *Leaving the harmonic basin*: starting from a local minimum, the configuration is deformed along a direction chosen randomly in the 3N-dimensional space until the lowest eigenvalue of the Hessian becomes negative.
(2) *Converging to a saddle point*: the system is pushed away from the initial minimum along the eigendirection corresponding to this negative eigenvalue, while the energy in the perpendicular hyperplane is minimized. The convergence is reached when the total force (parallel and perpendicular to the eigendirection) norm is below a given threshold. This is the transition state, a saddle point on the PES.
(3) *Relaxation stage*: after pushing the configuration over the saddle point, the energy is minimized using any standard minimization algorithm.

At the end of each ART event the resulting configuration, which minimize the total energy, can be accepted or rejected according to a Metropolis criterion, based on the energy difference between consecutive local minima, as described in Ref. 7. If the new configuration is accepted, the next event is started from the new configuration, otherwise it is started from the previous minimum.

In its original implementation, ART nouveau uses the Lanczós algorithm for determining the lowest eigenvalue of the Hessian and its corresponding eigenvector necessary in its first two stages. Because of the recursive application of the method, it was shown that only 15–20 force evaluations provide an accurate value of the lowest eigenvalue,[8,21] without the necessity to compute and diagonalize at every step the 3N-dimensional Hessian, an $\mathcal{O}(N^3)$ operation.

In this implementation, we have taken advantage of the recursive nature of the Lanczós procedure even further. We have observed that from one ART step to the next, the direction of the eigenvector changes very little. In most cases, the old and new eigenvectors are almost collinear. We have therefore chosen to compute only 13–16 force evaluations (8–10 in an empirical potential description of the forces) at a time and to repeat this procedure iteratively until we obtain an eigendirection parallel to the previous iteration. Not only is this method faster than former implementations, it is more robust to quirks in the energy landscape. Finally, we note that even with this small number of vectors, the application of a Gramm-Schmidt orthogonalization procedure is necessary to limit ghost states.

In the next subsections, we show how to reduce systematically the number of force evaluations during the activation stage while converging with a much greater precision onto the saddle point.

A. Direct inversion in the iterative subspace

The efficiency of the ART method is mostly dependent on the number of force evaluations required to successfully reach a saddle point. While numbers are often given for a single successful event, evaluation of the real costs requires taking into account both the average number of force evaluations needed to reach a saddle point and relax to a new minimum during a successful event and those lost in events that never converge onto a saddle point or never move to a new final minimum. It is necessary, therefore, to both minimize the number of force evaluations for reaching a saddle point and the fraction of failed events. When combined with the Lanczós algorithm, the DIIS method, proposed by Pulay,[26,27] is a technique that allows us to improve considerably both of these aspects at the same time.

The DIIS is a widely used approach for accelerating convergence both in the electronic structure and geometry optimization problems. However, in its original formulation, the DIIS procedure is assured to converge to the closest critical point, which can corresponds to different situations, e.g., saddle points, shoulders, or minima as shown in Fig. 1. This non-univocal behavior is a drawback in an energy minimum optimization process. Still, it can be turned into an advantage when one is interested in other critical points, a saddle point in our case, provided that DIIS is used with sufficient care.

In addition to its convergence properties, DIIS is also much less demanding that Lanczós in terms of force evaluation per step. While it is not possible to get away with much less than 15 force evaluations per step with the latter, DIIS demands only one, a crucial advantage when calculating the energy and forces is costly.

We propose thus a methodology combining both techniques to leverage the stability of Lanczós away for the
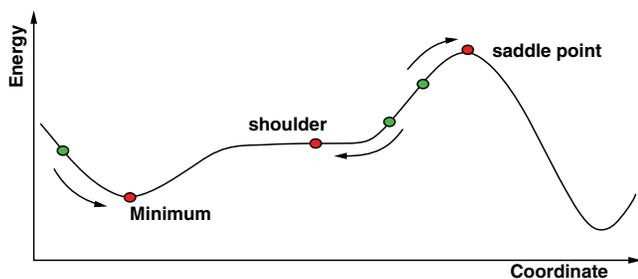
FIG. 1. A potential energy curve illustrating all critical points on where DIIS can converge. Green and red circles, respectively, initial configurations and converged critical points.

saddle point and the efficiency of DIIS near it. More precisely, our current Lanczós approach is used to bring the system out of the harmonic minimum and along the direction of negative curvature until the system is in the vicinity of a saddle point. The DIIS is then switch on, allowing a fast convergence to the saddle point in terms of the number of force evaluations.

A complete description of DIIS can be found in the literature.[28,29] For completeness, a short overview of the method is presented in the Appendix. In the following part we will describe with some detail our implementation.

B. Implementation

Our implementation of DIIS follows the scheme proposed by Farkas and Schlegel[28] for geometrical optimizations. For efficiency reasons, however, we use a diagonal approximation of the inverse Hessian, i.e., $\mathbf{H}^{-1} = \alpha\,\mathbf{I}$, where α is the size of the DIIS step. This approximation avoids explicit calculation of the Hessian, which would make this algorithm prohibitive for *ab initio* calculations.

This simplification has a cost, however, and it implies that important information about the curvature of the PES is not available for the convergence. In principle, an initial approximate Hessian can be constructed with the help of their n lowest eigenvalues obtained from the Lanczós method on a configuration near to the saddle point. This would provide a better approximation to the *residuum* vector, and therefore a better performance of the DIIS method. While such an approach could provide a significant boost in performance, the local nature of DIIS suggests that steepest descent is sufficient.

To be efficient, it is important to know DIIS limitations. Indeed, this algorithm is basically a quadratic approximation and its applicability should be limited to the quadratic region around the critical point. However, as pointed out by Farkas and Schlegel,[28] it is possible to circumvent these limitations and work outside the quadratic region by providing a set of criteria to control the procedure, in such a way that DIIS reliably converges towards a stationary point. Defined outside of the convergence radius, this set of criteria is somewhat *ad hoc*, of course, and should be tested and optimized according to the problem at hand.

The basic idea is simple, however, and works: whenever a given DIIS step provides a new structure $\mathbf{x}_{i+1}$ that does not

fulfill the acceptance criteria, the length of the DIIS memory is reduced, and a new configuration is generated and probed. In the present implementation two of the four original criteria[28] were used (see Appendix).

Figure 2 shows the evolution of the same generic event in C_{20} calculated with BigDFT, for the first two stages, i.e., *leaving the harmonic basin* and *converging to a saddle point* using a pure Lanczós approach (black line) or the mixed Lanczós+DIIS method proposed here.

Before comparing the convergence without and with DIIS, we first focus on the position of the arrow in Panel (a), which indicates the point where the configurations reach the edge of the harmonic basin—after 179 force evaluations, for this event—defined as showing a direction of negative curvature below a fixed threshold. Up to this point, the system is pushed in a random direction, exciting a number of modes in the Hessian. After this point, the convergence algorithm moves the configuration away from the minimum along the direction of negative curvature while relaxing the other $3N-1$ modes. The combination of relaxation on one hand and activation on the other causes the energy to evolve non-monotonically as it reaches the saddle point.

From the edge of the harmonic basin, the pure Lanczós algorithm brings the configuration along the eigendirection corresponding to the lowest negative eigenvalue up to the saddle point configuration. For this procedure, close to the saddle point, the energy tends to decrease, as the $3N-1$ excited modes relax, while the total force is being minimized, Panels (a) and (b). The process ends once the force falls below a given threshold (0.25 eV/Å), indicating that a saddle point has been reached. Since at each step, the number of force evaluations required in the Lanczós procedure (15) is four or five times larger than that needed for perpendicular minimization, the total number of force evaluations grows linearly with the number of steps and reaches 1488 at convergence.

In the mixed Lanczós+DIIS approach, both the energy and the forces do not decrease in a monotonically way once DIIS takes over (indicated by a vertical dashed line in Fig. 2). This is due to the fact that DIIS is an extrapolation method that treats all directions on an equal footing, making each iterative step much cheaper than with Lanczós. Since the direction of negative curvature is no longer special, we observe a significant gain in the number of force evaluations needed, which is clearly seen in the insets of Panels (a) and (b) and in the decrease of the slope for Panel (d). For this event, Panel (c), the DIIS method is launched four steps after the lower-eigenvalue of the Hessian has reached its latest minimum, as explained below.

C. Force convergence

While forces are formally exact with empirical potentials, they can be converged with various degree of precision in *ab initio* but, of course, at ever increasing computational cost. The stability of the algorithm as a function of force precision therefore impacts directly on its computational efficiency. Here again, DIIS has an edge over Lanczós. The
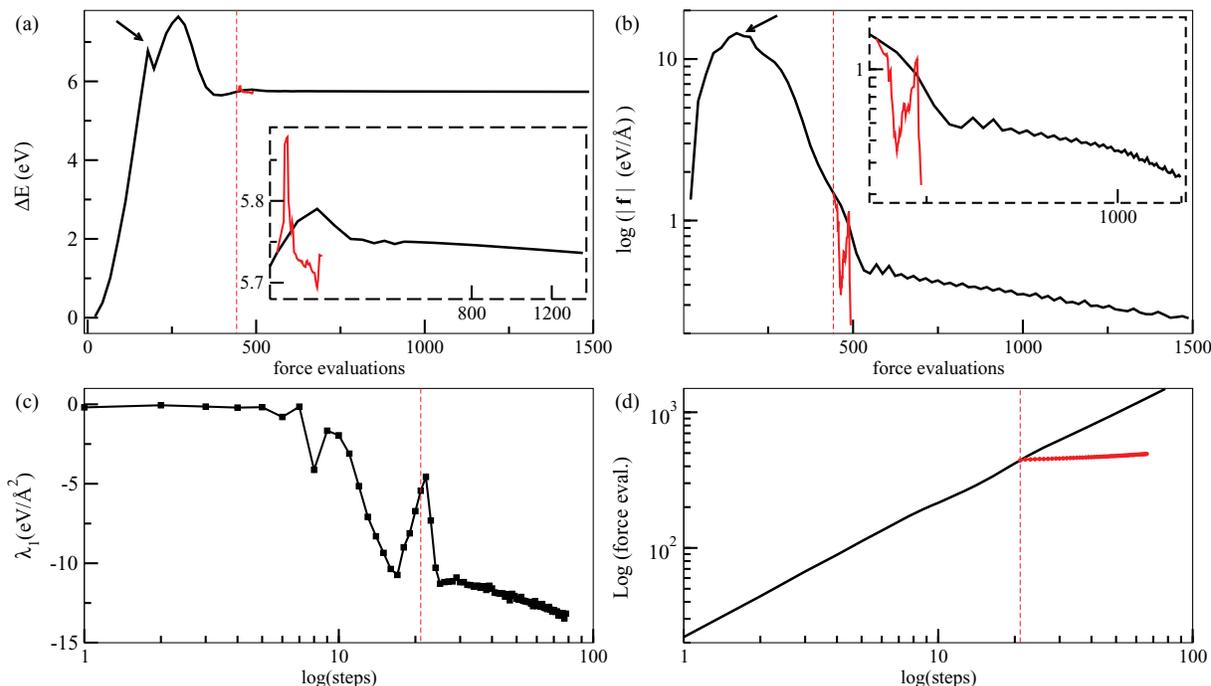
FIG. 2. Convergence to a given saddle point for C_{20} using a pure Lanczós scheme (black line) or the mixed Lanczós-DIIS method presented in this paper (red line). Panels (a) and (b) show the energy and the norm of the total force profiles as a function of the cumulative number of force evaluations. Panels (c) and (d) present the lowest eigenvalue and the number of force evaluations as a function of the step number. The arrows in Panel (a) and (b) indicate the transition in the ART nouveau algorithm from steps for leaving the harmonic well to a convergence towards the saddle point.

latter requires a numerical derivation of forces to construct the partial Hessian matrix.

Thus their convergence requirement directly impacts the ability of a given algorithm to obtain a stable and meaningful lowest eigenvalue and its corresponding eigenvector. We find that in the case of the Lanczós algorithm, it is necessary to converge the wavefunctions with a tolerance one order of magnitude higher than that used in DIIS as well as in geometry optimization algorithms. This leads to an increase of more than 60% for the number of steps in the wavefunctions convergence algorithm. As a result, for each force evaluation, the cost of the Lanczós algorithm is increased by 60% with respect to the DIIS algorithm.

Moreover, because *ab initio* convergence is more difficult away from the minimum, especially near a transition state, the gain is even greater for the region where DIIS is applied contributing again to the increase in efficiency for the algorithm presented here.

D. Statistical characterization

To fully ascertain the efficiency gain of this approach over the standard ART nouveau algorithm, we first turn to a 1000-atom model of amorphous silicon (a-Si) generated with ART nouveau and described with a modified Stillinger-Weber empirical potential.[15] This low-cost model allows us to obtain extensive statistics on the real impact of these modifications. For each set of parameters in our study, three independent simulations of 1000 successful events have been carried out.

Because of the numeric character of the method and to the fact that the initial activation is done in a random fashion, ART nouveau does not guarantee that every attempted event

converges to a saddle point. Thus, these failed events, together with the successful ones, should be also taken into account in a performance study. Moreover, some of the saddle points found are, in fact, only a shoulder inside a basin. In this case, the final minimum corresponds exactly to the original one. Such closed trajectory should not be counted either as a real event. Thus, our performance criterion takes into account both the number of force evaluations required for the three stages of a event and the number of real new configurations identified along a given trajectory.

These statistics averaged on three independent 1000-event trajectories are summarized in Table I, for both pure Lanczós and Lanczós+DIIS. On average, using only the original Lanczós implementation, about 5 168 000 force evaluations and 2889 attempts were necessary to generate 1000 successful events for each trajectory. Of these events, only 5% turned out to have sampled shoulders instead of real saddle points connecting two basin and 95% of the successful events are real new events.

We implemented the Fast inertial Relaxation Engine (FIRE) method,[30] a state-of-the-art minimization algorithm. Our original variable-step steepest descent method needed ~450 force evaluations to converge to the new minimum, while the FIRE algorithm needs about 45. The mixed Lanczós+DIIS simulations presented here also use the FIRE algorithm.

Launching mixed Lanczós+DIIS simulations requires first to define a criterion for switching from one convergence algorithm to the other. While there is no well-defined criterion, we have observed that, in general, the system reaches the neighborhood of a critical point after the lowest-eigenvalue of the Hessian has passed through a minimum in value. To

TABLE I. Amorphous silicon (*a*-Si): Statistic of the number of attempted and new (with respect to previous minimum) events obtained from three independent trajectories of 1000 successful events, each one using Lanczós+DIIS, as a function of the number of the Lanczós steps after the minimum in the lowest eigenvalue of the Hessian before launching DIIS (see text for details). Symbol ∞ means that only Lanczós method was used. For the ∞+FIRE and the simulations with DIIS, FIRE was used for relaxing from the saddle to the final minimum. The average number of force evaluation per successful event, $\langle f \rangle_s$, is obtained by dividing the total number of force calls needed to generate 1000 successful events by this number.

Steps after minimum	∞	∞+FIRE	10	4	2
$\langle f \rangle_s$	5168	4885	689	670	653
Attempted events	2889	3021	2487	2650	2571
New events	949	964	968	971	965

ensure that this minimum is significant and not a mere fluctuation, we impose that the slope in the change of this eigenvalue remains positive for a given number of Lanczós steps after this minimum, before launching DIIS (see, e.g., Fig. 2(c)). The impact of this present number of Lanczós steps after a minimum is presented in Table I. We do not observe a clear decrease of the failed events as the number of steps increases, indicating that Lanczós takes us efficiently in the region near the saddle point.

Since DIIS can converge to any critical point, not just saddle points, we also observe that early launch of DIIS leads to an increase in the number of events going back to the initial minimum in some circumstances. However, Lanczós is costly and a longer use implies an increasing number of force evaluations. A careful balance must, therefore, be reached between decreasing the number of force calls and a high convergence rate to real saddle points. Because of this, we prefer requiring 4 Lanczós steps with a positive slope for the lowest-eigenvalue before calling DIIS. This choice of parameter guarantees that most converged critical points are real saddle points under most circumstances. On average, using only Lanczós+DIIS, about 670 000 force evaluations and 2650

attempts were necessary to generate 1000 successful events for each trajectory. And with a cost per new event, when the cost of all attempted and failed events is included, about seven times smaller than with the Lanczós original algorithm, which represent a significant increase in overall efficiency.

III. THREE APPLICATIONS OF ART NOUVEAU WITH BIGDFT

While the large scale statistical analysis with an empirical potential of the Lanczós+DIIS scheme shows the clear advantage of this method, it is important to confirm that the method is applicable to systems described with an *ab initio* method. Here, we select BigDFT, a real-space wavelet-based DFT approach package with extremely efficient scaling, allowing the study of relatively large systems with a variety of boundary conditions.[31,32] We focus on three test systems: a cluster of C_{20}, a vacancy in bulk silicon, and a $(2 \times 2)_C$ reconstruction at the surface of a 4H-SiC slab.

In Table II, we summarize the set of *ab initio* conditions to the three systems studied here and the overall efficiency of the method. We note, in particular, that the number of force evaluations per event is significantly smaller than for the empirical potential, due to the smoother energy landscape associated with *ab initio*.

A. Defects in C_{20} clusters

As a first test case, we apply our activated scheme to a molecular system for which BigDFT has proven to be efficient for a large variety of systems, e.g., $C_{59}Pt$,[33] $Si_{30}C_{30}$ (Ref. 34), and B_{80}.[35] Here, we restrict ourselves to a small number of atoms, a cluster of 20 carbon atoms, C_{20}. Although this molecule counts only a small number of degrees of freedom, the exploration of its PES by an *ab initio* method can be a demanding task, if the study is not limited to small region of its configuration space.

TABLE II. Comparison between various saddle point converging algorithms. ART nouveau refers to the algorithm presented here and applied to *a*-Si with Stillinger-Weber potential as well as three systems studied with *ab initio* method. Results on Pt(111) surface for ARTn (Olsen) and Dimer method are from Ref. 51. The modified dimer methods applied, with various *ab initio* schemes, to a small organic molecule (Ref. 52) and a peptide in water (Ref. 53). The double-ended growing string method (GSM) is used to find the transition state for H-transfer in methanol oxidation in VO_x/SiO_2 (Ref. 54). BC refers to boundary condition: bulk, isolated, surface, or solution. DOF is the number of degrees of freedom available for each simulation. $\langle f \rangle$ is the number of force evaluations needed to go from a local minimum to a connected saddle point for a successful trajectory, while $\langle f \rangle_s$ is obtained by dividing the total number of force calls in a simulation by the number of successful events. A/S gives the total number of attempted over the number of successful events in the simulation presented here.

Algo.					ARTn (Olsen)				Improved dimer		GSM
Ref.		ART nouveau			51		Dimer method		52	53	6
System	*a*-Si	V_{Si}	C_{20}	SiC	Pt(111)	Pt(111)	Pt(111)	Pt(111)	C_6H_{10}	PHBH/H_2O	VO_x/SiO_2
BC	Bulk	Bulk	Isol.e	Surf.	Surf.	Surf.	Surf.	Surf.	Isol.	Sol.	Isol.
Pot.	SW	DFT	DFT	DFT	Morse	Morse	Morse	Morse	DFT	QM/MM	DFT
Method		PBE	LDA	PBE					B3LYP	AM1	B3LYP
DOF	3000	645	60	222	3	525	3	525	48	144	90[a]
$\langle f \rangle$	235	210	322	262	145	372	204	335	384[b]	425[c]	330
$\langle f \rangle_s$	670	302	718	728	145	2163	204	2148	...	...	...
A/S	2.72	79/78	434/201	134/75	...	...	...	...	...	...	...

[a]Estimated number of degrees of freedom.
[b]Starting near the saddle point and not from a minimum.
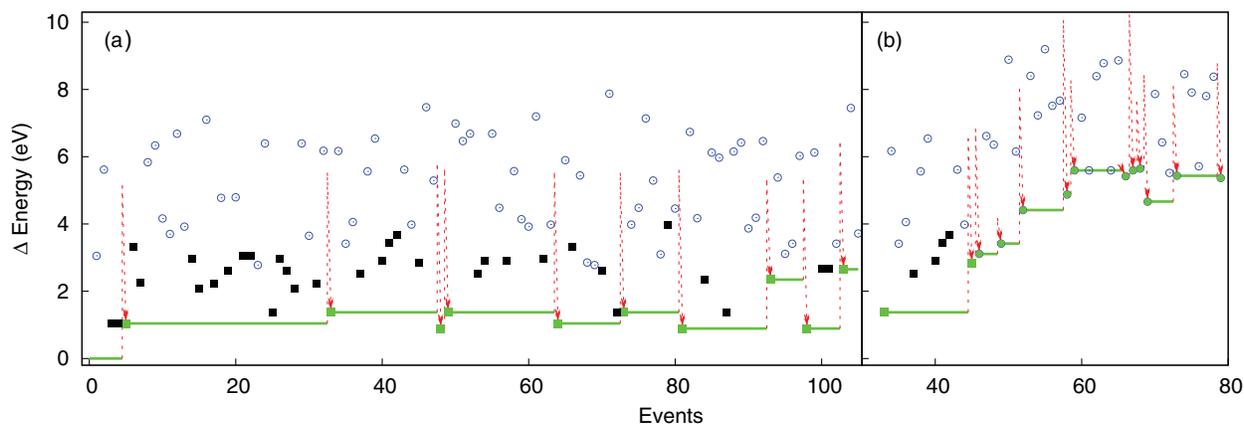[c]Approximate number extracted from Fig. 4 of Ref. 53; starting near the saddle point not from a minimum.

FIG. 3. Exploration of C_{20}'s potential energy surface: Energy difference (Δ energy) between each new relaxed structure (an event) and the total energy of the perfect C_{20} fullerene (zero event). Horizontal full lines and green symbols represent the energy of those configurations accepted by the Metropolis test. Filled squares and open circles represent, respectively, closed and open configurations. For clearness, only the Δ energy of the transition states of accepted events is drawn with dashed arrows. Metropolis temperature for (a) and (b) is 0.5 and 0.9 eV, respectively. In (b) green circles, accepted open configurations.

Experimental work on this cluster has shown that it can display a rich variety of structures including cages, bowls, graphene-like planes, rings, and linear chains.[36–39] From theoretical calculations, three of these structures can be considered as low-energy forms of C_{20} clusters: the planar ring, a curved graphitic bowl, and a closed-cage icosahedral fullerene. We have worked here within the local-density approximation (LDA) even though quantum Monte Carlo simulations suggest that this level of approximation leads to the wrong order in terms of the most stable structure for C_{20}.[40] Nevertheless, there is still no consensus about which is the most stable structure as the energy order of the three geometries depends strongly on the level of approximation used for the *ab initio* energy calculation. This question will be analysed in detail in a forthcoming publication.

In our simulations, we limit ourselves to the study of the configuration space around the closed-cage fullerene structure which is known to be the global minimum in LDA.[40] It is made only of 12 pentagons, thus the C_{20} cage is the smallest fullerene possible,[39] see Fig. 4(a). An interesting question regarding this C_{20} fullerene is whether it is possible to have other closed structures related to each other by Stone-Wales-type transformations as it is the case of C_{60}. Stone and Wales[41] have shown that other structures than the icosahedral one are possible for the C_{60} isomer by interchanging the positions of two hexagons and two pentagons. In these transformations, two sigma bonds are broken and are replaced by two new ones. In the particular case of C_{20}, this type of transforma-

tion will lead necessarily to a reduction of the pentagons rings through the creation of four- and six-membered rings and the molecule will lose its fullerene characteristic.

In order to sample the activated mechanisms associated with Stone-Wales-type distortions, we use a local initial-deformation vector, centered on one atom picked at random and its nearest neighbors defined as those within a radius of 1.5 Å. Figure 3(a) represents the ART exploration done on this system starting from the perfect C_{20} fullerene, with a fictitious Metropolis temperature of 0.5 eV. Each newly generated configuration is classified in terms of its open or closed character. The topological criterion for this determination is as follows: In a closed cluster every carbon atom is bonded to three others, while in an open system, the coordination of at least one atom is lower than three.

Figure 3(a) shows an extensive sampling, with more than 100 events, of the PES around the C_{20} fullerene. Although some open structures are observed along the simulation, the low fictitious temperature of the Metropolis test confines the exploration to the configuration space of closed structures. At least 14 closed and 41 open distinct structures were obtained. In general, closed configurations are lower in energy with respect to the open ones (the energy of closed configurations ranging between 0.9 and 3.7 eV above that of the C_{20} fullerene, while the open ones are at least 2.8 eV above). Figures 4(b), 4(c), and 4(d) show the three lowest energy structures observed along this ART exploration. The structure depicted in Fig. 4(b) is the result of one Stone-Wales

(a)$\Delta E=0.0$ eV   (b)$\Delta E=1.04$ eV   (c)$\Delta E=1.37$ eV   (d)$\Delta E=0.89$ eV   (e)$\Delta E=5.36$ eV
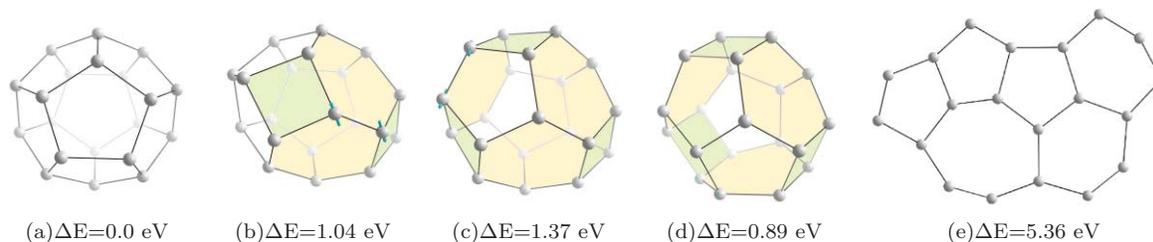
FIG. 4. C_{20} clusters: (a) Perfect C_{20} fullerene. (b)–(d) The three lowest energy structures and their energy difference with respect to the perfect C_{20} fullerene. For clarity, tetragons and hexagons are emphasized by shaded green and yellow colors. (e) A planar structure found along the simulation.

transformation on the perfect C_{20} fullerene: four pentagons are destroyed forming two tetragons and two hexagons, increasing the total energy by 1.04 eV. A second Stone-Wales transformation (Fig. 4(c)), on the latter structure, breaks another two pentagons and one tetragon generating a configuration with three hexagons, three tetragons, and six pentagons, increasing again the total energy by 0.33 eV. Finally, another Stone-Wales transformation, on the latter structure, leads to an arrangement of the three hexagons and three tetragons in a ring shape, with three pentagons at each side for forming the cage. This structure is stabilized by its higher symmetry and falls by almost 0.5 eV compared to the previous structure with an energy only 0.80 eV above the fullerene one.

Figure 3(b) presents an exploration of PES with a higher Metropolis temperature (0.9 eV), allowing a better sampling of opened structures. Here, we start from the structure shown in Fig. 4(c), with an energy 1.37 eV above the minimum. With a higher temperature, we see that the exploration moves rapidly to sample less stable higher energy configurations with respect to the fullerene cage, strongly favoring open-cage and even planer structures as that depicted in Fig. 4(e).

In conclusion, using ART-BigDFT, we were able to identify all the low-energy structures that emerge from the sequential application of Stone-Wales-type transformations in the perfect C_{20} fullerene. Using the mixed Lanczós+DIIS scheme, only 718 force evaluations were needed on average to generate a successful event, allowing us to get five events per day working with 40 cores and in a Message Passing Interface (MPI) scheme.

B. Vacancy diffusion in silicon bulk

We now move to a system with a large number of degrees of freedom, a 215-atom *c*-Si bulk system with a single vacancy, increasing the computational effort required for each *ab initio* force evaluation. Because we are only interested in events associated with the vacancy, the effective PES is simpler than for the C_{20}, as only the vacancy's nearest-neighbors and their surroundings are directly involved in the diffusion process.

Here, we focus more precisely on the neutral vacancy diffusion in bulk silicon at zero pressure. This defect's diffusion mechanism has been extensively described in previous works.[19,42,43] It has been shown that this system can undergo three different low-energy activated mechanisms that can be characterized in terms of the local Jahn-Teller (JT) tetragonal structure distortion of the vacancy.

This symmetry-breaking allows the four vacancy nearest neighbor atoms be paired two by two, forming a threefold degenerate state ($JT^a : a \in \{x, y, z\}$) depending on the plane in which both pairs are located. The first activated mechanism (labelled hereafter α) leads to the migration of the JT_i distortion to a nearest-neighbor site, preserving the same orientation, $JT_i^a \rightarrow JT_j^a$. This is done by the jump of one of the nearest-neighbor atoms along a direction almost parallel to $\langle 111 \rangle$ towards the vacant site. At finite temperature, this mechanism's transition state corresponds to the so-called split vacancy configuration.[43] Nevertheless, at zero temperature this structure lies in a shallow well along the path of this
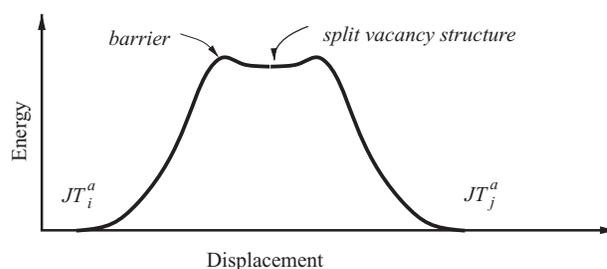

FIG. 5. Schematic representation of the total minimum-energy path for the simple diffusion at zero temperature. The intermediate minima is localized at ~ 0.04 eV and ~ 0.24 Å with respect to the barriers.

transition, see Fig. 5. A state which is easily smeared out by the thermal vibrations at room temperature. There is no diffusion either for the vacancy in the second activated mechanism, but a reorientation of the JT distortion. This corresponds to a rotation of the JT tetrahedron, $JT_i^a \rightarrow JT_i^b$ (labelled hereafter, β if $a \neq b$ and γ if $a = b$), due to the rearrangement of the atoms pairs in it. Finally, one combination of previous mechanisms can lead to the migration of the JT distortion, together with its reorientation, $JT_i^a \rightarrow JT_j^b$ (labelled hereafter δ).

Figure 6 shows the sampling of activated mechanisms related with the vacancy for our simulations, where only initial local deformations centered on the atoms surrounding are applied. All events are started at a lowest-energy state JT_i^a. During sampling, we find successfully all mechanisms described above. The average value of the activation energy for the diffusion mechanism (α and δ) and the reorientation mechanism (β and γ) are, respectively, 0.32 and 0.27 eV, in good agreement with previous studies.[42,43] The spreading around these average values is connected to the DIIS convergence criteria used in the present exploration, as illustrated in Fig. 6 where this criterion was reduced after event number ten. In addition, due to the fact that we are working at zero temperature, some events fell in the intermediate minima between two JT configuration, i.e., in the split vacancy structure.
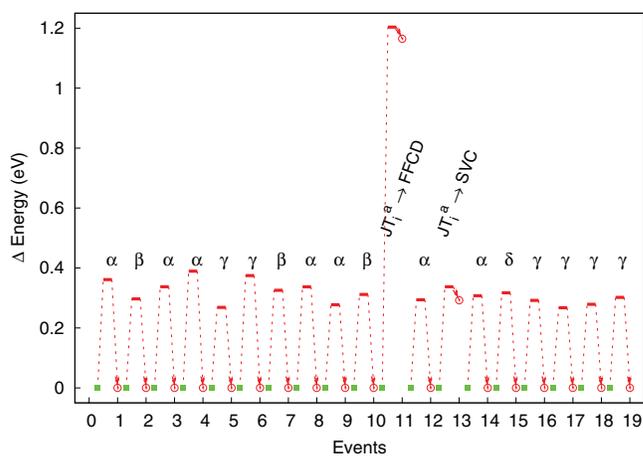

FIG. 6. Sampling of activated mechanisms related with the vacancy. Energy difference for each event is measured with respect to the energy of the relaxed vacancy. $\alpha = JT_i^a \rightarrow JT_j^a$, $\beta = JT_i^a \rightarrow JT_j^a$, $\gamma = JT_i^a \rightarrow JT_i^b$ and $\delta = JT_i^a \rightarrow JT_j^b$
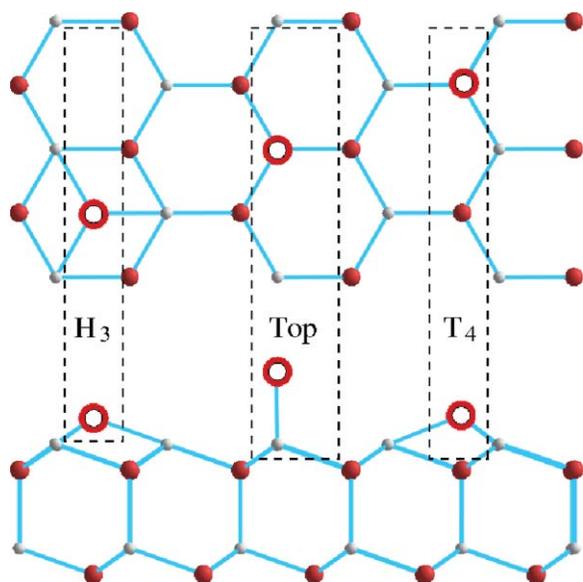
FIG. 7. Top and side view of the SiC $(000\bar{1})$ surface with the three possible high-symmetry positions of the adatom (white ball).

As we shown in Fig. 6, we have also observed high-energy transition events that involve complex atomistic rearrangements.[16,19] This event corresponds to the bond-exchange move proposed by Wooten *et al.*[44] as a mechanism for amorphization and leads to the fourfold coordinated defect.[45]

Regarding the computational cost, on average, each successful event demands 302 force evaluations. This reduction of 42%, with respect to the 700 force evaluations necessary in a previous *ab initio* ART exploration,[19] is in the line of the 33% reported above for *a*-Si. Indeed, in the previous *ab initio* ART exploration (i.e., with pure Lanczós method) the force calculations for unsuccessful events were not included in the latter's number.[19] The more efficient activation algorithm coupled with the highly parallelizable BigDFT allows us to generated up to five events per day for this system using 430 cores in a MPI paralllization scheme.

C. Reconstruction of 4H-SiC surfaces

Finally, we consider a surface reconstruction of SiC, a system of intermediate size but with a rich dynamics. In this type of system, the number of atoms involved in the rearrangement of the surface, essentially the atoms on the top layer and, sometimes, those below, determine a large sector of the energy landscape to be explored. Here, we focus on the $(2 \times 2)_C$ reconstruction of the 4H hexagonal polytype of SiC, a system of great interest nowadays.[46–48]

The structural description of the atoms in the $(2 \times 2)_C$ reconstruction of the SiC $(000\bar{1})$ is quite puzzling: after Si sublimation of the sacrificial layer, a 2×2 cell does have four dangling bonds (DB), one per surface C atom. Experimentally, Seubert *et al.*[49] found evidence of an adatom per unit cell in the surface, which should reduce the electronic instability due to the DBs. This adatom is likely localized in

one of the three high-symmetry positions of the surface H_3, T_4, and top (see Fig. 7). A model of a silicon adatom in position H_3, such it occupies a three-fold coordinated hollow site, appears as the model with better agreement with the experimental evidence. In a recent work Magaud *et al.*[50] supported this hypothesis with an *ab initio* study on the three proposed structures. They observed that a Si atom in H_3 site is around 1.12 eV more stable than that in a T_4 site, and the *top* is found to be more than 2.0 eV higher than the former.

Here with the help of ART, we sampled the PES in a more exhaustive way. Contrary to the work of Magaud *et al.*, we do not have to impose any constraint on the symmetry, allowing us to get insight about the possible diffusion mechanisms of the atoms at this kind of surface. Instead of using the conventional $(2 \times 2)_C$ representation with one adatom only per unit cell as was done by Magaud *et al.*, we considered an orthorhombic cell representation with two adatoms per unit cell. We launched a set of independent simulations to sample the energy landscape around three configurations (both adatoms being in the same configuration) with a Metropolis temperature 0.5 eV. Initial activations were performed using only initial local deformations, centered at random on one superficial atom, with a radius of 2.5 Å.

The barriers sampled in our simulations are represented in Fig. 8. In agreement with a previous result,[50] the most stable structure arising from the exploration is a configuration where both adatoms are in H_3 sites, about 2.6 eV below the T_4. The energy discrepancy with respect to previous calculations (2.24 eV for two adatoms) has been verified to be due to the use of Γ point only during the exploration. In our simulations pure T_4 configurations have a very unstable character. Indeed, this configuration appears as a saddle configuration in the migration mechanism of the adatoms between two H_3 sites. Moreover, we never observed a configuration consisting of both atoms in top sites as a local minimum as far all the simulations starting from this configuration relaxed in to a H_3 symmetry. As we see in Fig. 8, less stable minimum other than the H_3 one were observed; however, they do not conserve the experimental symmetry of the observed $(2 \times 2)_C$ reconstruction. One of these structures the H_3T_4 configuration appears to be an intermediate configuration for migration of adatoms over the surface.

This mechanism can be described as a collective migration of both adatoms along the $\langle 10 \rangle$ surface direction in to the corresponding neighbor H_3 site. Starting from both adatoms in H_3 configuration, event $E_0(H_3H_3)$ in Figs. 9 and 10, it follows $E_2(H_3T_4) \rightarrow E_3(T_4H_3) \rightarrow E_4(H_3H_3)$. The configuration of the transition state between E_2 and E_3 minima is close to a T_4 symmetry (see Fig. 10). We should note, however, that the energy barrier for this mechanism is high and that it has a low-probability at low temperatures.

In conclusion, using ART-BigDFT we were able to identify the low-energy structures of the silicon adatoms on top of the reconstructed $(2 \times 2)_C$ SiC surface as well as their surface diffusion pathway. On average, one successful event demands 728 force evaluations and we get four events per day working with 136 cores in a MPI paralllization scheme.
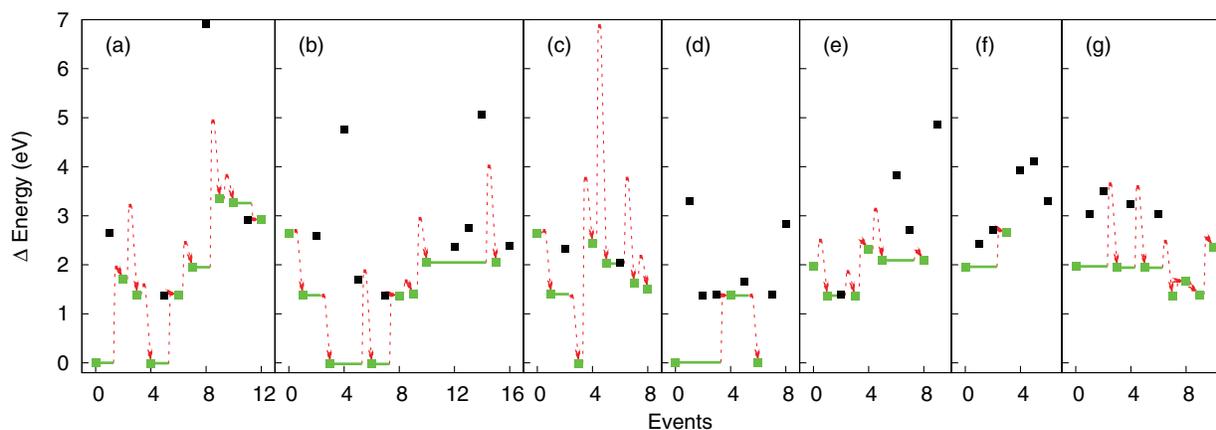
FIG. 8. Seven independent exploration of 4H-SiC's PES: Energy difference of each event with respect to the total energy of the H_3 symmetry configuration. Green full lines and squares, accepted configurations, red dashed lines, transition states, black square symbols, rejected events. For clearness, only the Δ energy of the transition states of accepted events is drawn with dashed arrows.

IV. COMPARISON WITH OTHER METHODS

It is possible to compare this version of ART nouveau with other algorithms. An extensive study by Olsen *et al.* has shown that with the same method, an increasing number of degrees of freedom makes convergence to the transition much more difficult.[51] With the same parameters, for example, ART nouveau as implemented by Olsen *et al.* takes, on average, only 145 force evaluations to converge to an adjacent saddle point when a single atom is allowed to move on a frozen surface, while it takes about 930 force evaluations when seven atoms can move and 2163 with 175 free atoms. This is generally what we observe here as shown in Table II, if we take into account the effective number of degrees of freedom: the number of force evaluations required to converge to a saddle point in the case of vacancy diffusion in *c*-Si, with four atoms that can diffuse in the void, is only 210, while it is 262 for diffusion on a SiC surface, where half the atoms are buried, and 322 in C_{20}, where all atoms participate in events. Since the effective size of events, i.e., the average number of atoms involved in an event, saturates with increase in system size, Olsen *et al.* found that, although methods using an exact Hessian calculations were significantly more efficient for low-dimensional systems, in all cases, the dimer and ART nouveau methods were preferable in high-dimensional systems, especially when sampling a large number of transition states was needed.

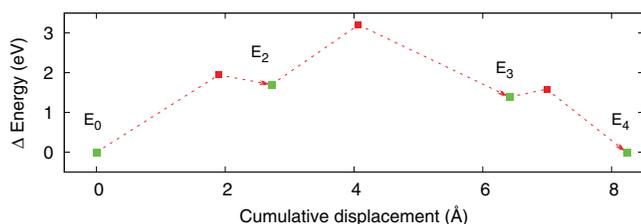We observe a similar situation when looking at the global reaction route mapping (GRRM) by Ohno and Maeda,[12] a

FIG. 9. Δ of energy with respect of the cumulative displacement between the events E_0, E_2, E_3, and E_4 in Panel (a) of Fig. 8. Green squares, minimum configurations, red dashed lines, transition states.

systematic approach for finding transition states, which requires the full search for pathways through a hypersphere around a local minimum. Even for the smallest system studied in Ref. 55, H_2CO, including Hessian calculations, the algorithm requires a total of 14 600 force evaluations to find all nine pathways, a number that increases rapidly with size and which corresponds to more than 20 successful ART events. If GRRM could be preferable for small systems, ART nouveau and similar methods are clearly favored with increasing number of degrees of freedom.

Table II compares the efficiency of the current implementation of ART nouveau combined with empirical and *ab initio* forcefield to the results obtained by Olsen *et al.* with the dimer method and their own implementation of ART nouveau. In both cases, results are for an open-ended search. We also compare with the double-ended growing string method by Goodrow *et al.*[6] as well as recent versions of the dimer method,[10] that of Heyden *et al.*[52] and that Kästner and Sherwookd,[53] which are applied this time to double-ended problems. Neither of these works start from a local minimum, simplifying convergence to a transition state as compared with an unbiased search as with ART nouveau. In the first case, an initial pathway is constructed using the growing string method[4] and the dimer method is used to refine the configuration closest to the transition state.[52] In the second case, the method is tested starting from various points on a previously generated reaction trajectory.[53]

Overall, when using an empirical potential, which allows a more accurate calculation of the force's first derivative, ART nouveau requires about 235 force evaluations to converge to a nearby transition state compared with 335 with the dimer method of Olsen *et al.*[51] The improvement is even more significant when including the full cost of missed events and the final minimization. In this case, ART nouveau with about 670 force calculations is more than three times faster than the dimer.

Similarly, with *ab initio* forces, BigDFT-ART results, even starting from a local minimum, show a 20%–30% efficiency gain as compared with the work of Heyden *et al.*[52] and Käster and Sherwood.[53] Removing the force calculations
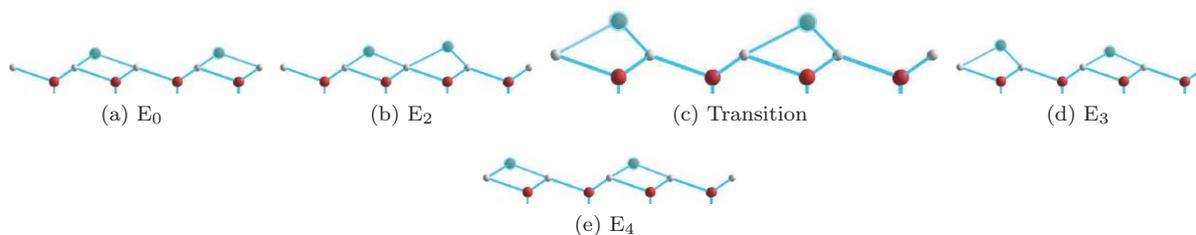
FIG. 10. Schematic representation of the events depicted in Fig. 9. $E_0(H_3H_3)$, $E_2(H_3T_4)$, $E_3(T_4H_3)$, and $E_4(H_3H_3)$.

needed to leave the harmonic basin in ART nouveau simulations, about 70%–80%, we find rather a 55%–70% gain in efficiency. Comparing with results of Goodrow *et al.* with the diffusion of a vacancy in Si, a system with a comparable effective number of degrees of freedom, we note that, even open-ended, BigDFT-ART is about 60% faster.

V. CONCLUSIONS

Open-ended saddle point methods provide a simple way to sample the energy surface and reaction pathways for complex systems, from molecules to bulk and surfaces. These methods can be costly; however, which is why they were not regularly used for finding transition states and pathways.

In this paper, we revisit the basic algorithm behind the activation-relaxation technique (ART nouveau), introducing a two-step convergence to the saddle point, first with the previously used Lanczós scheme and turning to DIIS near the transition state. This modification allows us to improve the efficiency of the algorithm, in terms of the required number of force evaluations, by a factor of 3, to a little more than 300 in certain cases, a crucial improvement for coupling this method with *ab initio* packages. It also provides a more stable algorithm, that requires fewer adjustments to new systems and can work, for the most part, with less stringent convergence on the forces, decreasing further its computational cost.

The improvements presented here should make systematic unbiased studies of diffusion mechanisms very competitive even with more traditional approaches where pathway are first guessed before being refined, such as NEBM, while providing an unbiased search for mechanisms.

More important, the efficiency of this mixed algorithm is demonstrated, coupled with BigDFT, on a number of problems that go beyond saddle-point refining: sampling the potential energy surface of C_{20}, the self-diffusion mechanisms of a V_{Si} in bulk c-Si and finding reconstruction pathways at the surface of SiC. This opens up the possibility of applying on a regular basis this type of extensive unbiased search for activated events and low-energy structures more systematically to systems needing *ab initio*-level description.

ACKNOWLEDGMENTS

APPENDIX: DIIS METHOD

In a geometry optimization context, DIIS can be seen as a linear interpolation (and extrapolation) of a previously known set of structures $\{\mathbf{x}_i\}$ (the DIIS memory) that minimize the norm of a *residuum* $\mathbf{r}$ associated with the structure $\mathbf{x}^*$,

$$\mathbf{x}^* = \sum c_i \mathbf{x}_i, \quad \text{where} \quad \sum c_i = 1. \tag{A1}$$

Each structure $\mathbf{x}_i$ has an associated *residuum* vector $\mathbf{e}_i$ defined by the displacement

$$\mathbf{e}_i = \mathbf{x}_i^N - \mathbf{x}_i, \tag{A2}$$

where $\mathbf{x}_i^N$ is a *pure* Newton optimization step, i.e.,

$$\mathbf{x}_i^N = \mathbf{x}_i + \mathbf{H}^{-1}\mathbf{f}_i, \tag{A3}$$

where $\mathbf{f}_i$ is the force (negative of the total energy gradient) and $\mathbf{H}^{-1}$ the inverse Hessian (second derivative of the total energy) at $\mathbf{x}_i$. Thus, the *residuum* vector $\mathbf{e}_i$ is

$$\mathbf{e}_i = \mathbf{H}^{-1}\mathbf{f}_i. \tag{A4}$$

The coefficients c_i in Eq. (A1) can be obtained by assuming linearity in the *residuum* vector $\mathbf{r}$, i.e.,

$$\mathbf{r} = \sum c_i \mathbf{e}_i, \tag{A5}$$

and minimizing $|\mathbf{r}|^2$ such that $\sum c_i = 1$. This leads to the system of equations

$$\begin{pmatrix} a_{1,1} & \cdots & a_{1,i} & 1 \\ \vdots & \ddots & \vdots & \vdots \\ a_{i,1} & \cdots & a_{i,i} & 1 \\ 1 & \cdots & 1 & 0 \end{pmatrix} \begin{pmatrix} c_1 \\ \vdots \\ c_i \\ \lambda \end{pmatrix} = \begin{pmatrix} 0 \\ \vdots \\ 0 \\ 1 \end{pmatrix}, \tag{A6}$$

where each matrix element a_{ij} is defined as the product of individual *residuum* vectors, $a_{ij} = \mathbf{e}_i^T \mathbf{e}_j$ and λ is a Lagrange multiplier. The resulting geometry $\mathbf{x}^*$ is the one that minimizes the *residuum* $\mathbf{r}$ within the searching space $\{\mathbf{x}_i\}$. If the structure $\mathbf{x}^*$ is not the exact solution, a new structure is added to the memory as

$$\mathbf{x}_{i+1} = \mathbf{x}^* + \mathbf{r} = \sum c_i(\mathbf{x}_i + \mathbf{e}_i) = \sum c_i \mathbf{x}_i^N \tag{A7}$$

and the iteration is continued.

In the present implementation, we use as an acceptance criteria for a given DIIS configuration:

- The length of the DIIS step, i.e., $|\mathbf{x}_{i+1} - \mathbf{x}_i|$, is limited to be no more than five times α (see text). This reduces the odds of getting a new configuration too far from those that are in the memory. In addition, this improves the *ab initio* self-consistent field convergence over the accepted configuration, since the previously calculated wavefunctions can be used as input guess.

- If the magnitude of $\mathbf{c}/|\mathbf{r}|^2$ exceeds 10^8, the step is refused. This reduces numerical stability problems when the matrix $\mathbf{A} = \{a_{ij}\}$ becomes nearly singular.

[1] G. Henkelman, B. Uberuaga, and H. Jonsson, J. Chem. Phys. **113**, 9901 (2000).
[2] G. Henkelman and H. Jonsson, J. Chem. Phys. **113**, 9978 (2000).
[3] S. Trygubenko and D. Wales, J. Chem. Phys. **120**, 2082 (2004).
[4] B. Peters, A. Heyden, A. T. Bell, and A. Chakraborty, J. Chem. Phys. **120**, 7877 (2004).
[5] W. Quapp, J. Comput. Chem. **28**, 1834 (2007).
[6] A. Goodrow, A. T. Bell, and M. Head-Gordon, J. Chem. Phys. **130**, 244108 (2009).
[7] G. Barkema and N. Mousseau, Phys. Rev. Lett. **77**, 4358 (1996).
[8] R. Malek and N. Mousseau, Phys. Rev. E **62**, 7723 (2000).
[9] J. Doye and D. Wales, Z. Phys. D: At., Mol. Clusters **40**, 194 (1997).
[10] G. Henkelman and H. Jonsson, J. Chem. Phys. **111**, 7010 (1999).
[11] S. Goedecker, J. Chem. Phys. **120**, 9911 (2004).
[12] K. Ohno and S. Maeda, Chem. Phys. Lett. **384**, 277 (2004).
[13] N. Mousseau and G. Barkema, Phys. Rev. E **57**, 2419 (1998).
[14] G. Wei, N. Mousseau, and P. Derreumaux, Proteins **56**, 464 (2004).
[15] K. Houssem, N. Mousseau, and F. Schiettekatte, Phys. Rev. Lett. **105**, 045503 (2010).
[16] Y. Kumeda, D. Wales, and L. Munro, Chem. Phys. Lett. **341**, 185 (2001).
[17] L. Xu, G. Henkelman, C. Campbell, and H. Jonsson, Phys. Rev. Lett. **95**, 146103 (2005).
[18] J. M. Soler, E. Artacho, J. D. Gale, A. García, J. Junquera, P. Ordejón, and D. Sánchez-Portal, J. Phys.: Condens. Matter **14**, 2745 (2002).
[19] F. El-Mellouhi, N. Mousseau, and P. Ordejón, Phys. Rev. B **70**, 205202 (2004).
[20] F. El-Mellouhi and N. Mousseau, Appl. Phys. A **86**, 309 (2007).
[21] M.-C. Marinica, F. Willaime, and N. Mousseau, Phys. Rev. B **83**, 094119 (2011).
[22] K. Levasseur-Smith and N. Mousseau, J. Appl. Phys. **103**, 113502 (2008).
[23] L. Genovese, A. Neelov, S. Goedecker, T. Deutsch, S. A. Ghasemi, A. Willand, D. Caliste, O. Zilberberg, M. Rayson, A. Bergman, and R. Schneider, J. Chem. Phys. **129**, 014109 (2008).
[24] L. Genovese, M. Ospici, T. Deutsch, J-F. Méhaut, A. Neelov, and S. Goedecker, J. Chem. Phys. **131**, 034103 (2009).
[25] D. Wales and J. Doye, J. Phys. Chem. A **101**, 5111 (1997).
[26] P. Pulay, Chem. Phys. Lett. **73**, 393 (1980).
[27] P. Pulay, J. Comput. Chem. **3**, 556 (1982).
[28] O. Farkas and H. Schlegel, Phys. Chem. Chem. Phys. **4**, 11 (2002).
[29] R. Shepard and M. Minkoff, Mol. Phys. **105**, 2839 (2007).
[30] E. Bitzek, P. Koskinen, F. Gähler, M. Moseler, and P. Gumbsch, Phys. Rev. Lett. **97**, 170201 (2006).
[31] L. Genovese, T. Deutsch, and S. Goedecker, J. Chem. Phys. **127**, 054704 (2007).
[32] L. Genovese, T. Deutsch, A. Neelov, S. Goedecker, and G. Beylkin, J. Chem. Phys. **125**, 074105 (2006).
[33] M. A. Gabriel, L. Genovese, G. Krosnicki, O. Lemaire, T. Deutsch, and A. A. Franco, Phys. Chem. Chem. Phys. **12**, 9406 (2010).
[34] P. Pochet, L. Genovese, D. Caliste, I. Rousseau, S. Goedecker, and T. Deutsch, Phys. Rev. B **82**, 035431 (2010).
[35] P. Pochet, L. Genovese, S. De, S. Goedecker, D. Caliste, S. A. Ghasemi, K. Bao, and T. Deutsch, Phys. Rev. B **83**, 081403 (2011).
[36] G. Vonhelden, P. Kemper, N. Gotts, and M. Bowers, Science **259**, 1300 (1993).
[37] G. Vonhelden, M. Hsu, N. Gotts, and M. Bowers, J. Phys. Chem. **97**, 8182 (1993).
[38] H. Prinzbach, F. Wahl, A. Weiler, P. Landenberger, J. Wörth, L. T. Scott, M. Gelmont, D. Olevano, F. Sommer, and B. v. Issendorff, Chem.-Eur. J. **12**, 6268 (2006).
[39] H. Prinzbach, A. Weiler, P. Landenberger, F. Wahl, J. Wörth, L. T. Scott, M. Gelmont, D. Olevano, and B. v. Issendorff, Nature (London) **407**, 60 (2000).
[40] C. R. Hsing, C. M. Wei, N. D. Drummond, and R. J. Needs, Phys. Rev. B **79**, 245401 (2009).
[41] A. Stone and D. Wales, Chem. Phys. Lett. **128**, 501 (1986).
[42] K. Z. Rushchanskii, P. Pochet, and F. Lancon, Appl. Phys. Lett. **92**, 152110 (2008).
[43] D. Caliste, K. Rushchanskii, and P. Pochet, Appl. Phys. Lett. **98**, 031908 (2011).
[44] F. Wooten, K. Winer, and D. Weaire, Phys. Rev. Lett. **54**, 1392 (1985).
[45] S. Goedecker, T. Deutsch, and L. Billard, Phys. Rev. Lett. **88**, 235501 (2002).
[46] J. Hass, F. Varchon, J. E. Millán-Otoya, M. Sprinkle, N. Sharma, W. A. de Heer, C. Berger, P. N. First, L. Magaud, and E. H. Conrad, Phys. Rev. Lett. **100**, 125504 (2008).
[47] P. Mallet, F. Varchon, C. Naud, L. Magaud, C. Berger, and J.-Y. Veuillen, Phys. Rev. B **76**, 041403 (2007).
[48] F. Varchon, R. Feng, J. Hass, X. Li, B. Ngoc Nguyen, C. Naud, P. Mallet, J.-Y. Veuillen, C. Berger, E. H. Conrad, and L. Magaud, Phys. Rev. Lett. **99**, 126805 (2007).
[49] A. Seubert, J. Bernhardt, M. Nerding, U. Starke, and K. Heinz, Surf. Sci. **454**, 45 (2000).
[50] L. Magaud, F. Hiebel, F. Varchon, P. Mallet, and J. Y. Veuillen, Phys. Rev. B **79**, 161405 (2009).
[51] R. A. Olsen, J. G. Kroes, G. Henkelman, A. Arnaldsson, and H. Jónsson, J. Chem. Phys. **121**, 9776 (2004).
[52] A. Heyden, A. T. Bell, and F. Keil, J. Chem. Phys. **123**, 224101 (2005).
[53] J. Kästner and P. Sherwood, J. Chem. Phys. **128**, 014106 (2009).
[54] A. Goodrow and A. T. Bell, J. Phys. Chem. C **112**, 13204 (2008).
[55] S. Maeda, K. Ohno, and K. Morokuma, J. Chem. Theory Comput. **5**, 2734 (2009).